# Cyclic voltammetry of mono- and diiron(II)Cyclopentadienyl complexes of thianthrene and related heterocycles

R. Quin Bligh, Roger Moulton, Allen J. Bard, Adam Piorko, and Ronald G. Sutherland

## More About This Article

The permalink http://dx.doi.org/10.1021/ic00312a030 provides access to:

- Links to articles and content related to this article
- Copyright permission to reproduce figures and/or text from this article

nate-bond formation, not only for the metal–dioxygen bond but also for the coordinate bonds between the metal ion and the ligand donor atoms. The increase in the electropositive nature of the metal ion on oxygenation results in strengthening of its coordinate bonds, thus contributing considerably to the exothermicity of the reaction. All entropies of oxygenation are seen to be negative, a general characteristic for all oxygenation processes. The observed decrease of entropy is considered derived from two sources: (1) the loss of translational entropy of the oxygen molecule when it becomes bound and (2) the increase in rigidity of the ligand due to strengthening of the coordinate bonds, and consequent loss of vibrational and partial rotational freedom of the ligand.

Increasing the temperature seems to favor 2:1 complex formation (peroxo-bridged binuclear dioxygen complex). With bis(methylamino)pyridine as an axial base the CoSALOPHEN complex, **3**, forms a 2:1 complex at 25 °C; however, at 0 °C it forms a 1:1 complex.[7]

A review of the literature revealed that very little work has been carried out previously on the determination of oxygenation constants of cobalt Schiff bases complexes in solution. Surprisingly, there are no reports of oxygenation constants of CoFLUOMINE (**7**) in any solvent, although its solid–gas equilibrium has been very thoroughly investigated. Of the oxygen carriers for which oxygenation constants are reported in this paper, only in the case 3MeOSALTMEN has a solution oxygenation constant been reported by others. Baker et al.[12] reported the oxygenation constant log $K_{O_2}$ = –2.0), which is somewhat larger than the value reported in Table I, but this seems reasonable in view of the fact that it was measured at a lower temperature (–10 °C) and in the presence of a much stronger base. Also the solvent employed, $\gamma$-butyrolactone, was different. The only other comparisons that can be made with work in the literature involve the parent complex, **1**, which was described in both ref 7 and 12. Although the cobalt complex of 3MeOSALEN was described in both papers, only a very rough approximate value was measured in this work, because the constant was found to be concentration dependent, probably indicating a mixture of 1:1 and 2:1 dioxygen complexes. Baker et al.,[12] however, reported the 1:1 constant without comment. In our hands, and in diglyme solution, the parent complex **1** forms a 2:1 complex and therefore cannot be compared with the 1:1 constant reported by Baker et al.[12] For CoSALTMEN, the oxygenation constant found here for diglyme solution at 0.5 °C is very small, ca. –3.5, while the value reported[12] for DMAC solution at 5 °C is similar, ca. –3.4. These low values, which seem to be lower than those of any other cobalt Schiff base complexes reported, may indicate steric effects resulting from the distortion from planarity of the ligand by the four methyl substituents on the ethylene bridge.

All of the 23 oxygenation constants reported thus far for cobalt Schiff bases in solution are found in ref 7 and 12 and in this paper. They involve 16 Schiff bases, measured in five different solvents, with four different Schiff bases, and at several temperatures. In 12 cases, the temperature variation of the oxygenation constant was determined (this work and ref 7). When one considers the wide variation in the magnitude of the oxygenation constants reported, the presence of obvious steric effects, and the fact that the formation of 2:1 vs 1:1 constants is not yet predictable, it becomes apparent that at the present time there are insufficient data to develop dependable structure–stability relationships for these dioxygen complex systems.

The rates of degradation to inert complexes were appreciable for several complexes as noted above. A surprise was the observed degradation of CoFLUOMINE in diglyme solution, in view of the fact that the solid material may be recycled hundreds of times while maintaining most of its dioxygen carrier capacity. It is suggested that the mobility of dioxygen complexes in solution greatly facilitates degradation reactions to form inert complexes, implying that such degradation processes are bimolecular in nature. Similar effects have been observed for cobalt–dioxygen complexes with polyamine ligands in aqueous solution. Thus, the dioxygen complex of Co–DTMA (diethylenetriaminemonoacetic acid)[19] is stable for weeks in $10^{-3}$ solution but decomposes rapidly at $10^{-1}$ M concentration.

(19) McLendon, G.; MacMillan, D.; Hariharan, M.; Martell, A. E. *Inorg. Chem.* **1975**, *14*, 2322.

---

Contribution from the Departments of Chemistry, The University of Texas at Austin, Austin, Texas 78712, and University of Saskatchewan, Saskatoon, Saskatchewan S7N 0W0, Canada

# Cyclic Voltammetry of Mono- and Diiron(II) Cyclopentadienyl Complexes of Thianthrene and Related Heterocycles

R. Quin Bligh,[†] Roger Moulton,[†] Allen J. Bard,[*,†] Adam Piórko,[‡] and Ronald G. Sutherland[‡]

Electrochemical studies of mono- and diiron cyclopentadienyl complexes of thianthrene (TH), phenothiazine, and diphenylene dioxide at a platinum electrode in MeCN and $CH_2Cl_2$ solutions containing tetra-*n*-butylammonium hexafluorophosphate are reported. At fast scan rates (above 10 V/s) at an ultramicroelectrode (25-$\mu$m diameter) in MeCN, the diiron complexes show two Nernstian one-electron reduction waves. The small separation of the reduction waves (180 mV for the TH complex) is attributed to a moderate through-space interaction of the two Fe(cp) centers in the dimer. At slower scan rates, some decomposition of the reduced complex is observed; the chemical step involves cleavage of the Fe–arene bond to form the free arene and a solvated cpFe$^I$ species. This cpFe$^I$ species reacts with added CO to produce (cpFe(CO)$_2$)$_2$, disproportionates to form ferrocene and FeCO, or reduces the TH complex in homogeneous solution. Digital simulations of the electrochemistry are presented in support of the assigned mechanism. The monoiron TH complex displays similar reactions, with the TH(Fe$^I$cp) species more stable in $CH_2Cl_2$ than in MeCN solutions.

## Introduction

We report here the electrochemical studies of mono- and diiron cyclopentadienyl complexes of thianthrene, phenothiazine, and diphenylene dioxide. These diarenes have structures analogous

to anthracene, with the exception that positions 9 and 10 (i.e., the heteroatomic sites) are saturated. Coordination of the arenes to iron occurs through one (monoiron systems) or both (diiron systems) of the arene rings (Figure 1).

There have been numerous studies of ($\eta^6$-arene)($\eta^5$-cyclopentadienyl)iron(II) complexes that focus on electronic properties.[1-5] Unlike other iron(II) complexes, specifically the fer-

---

* To whom correspondence should be addressed.
† The University of Texas.
‡ University of Saskatchewan.
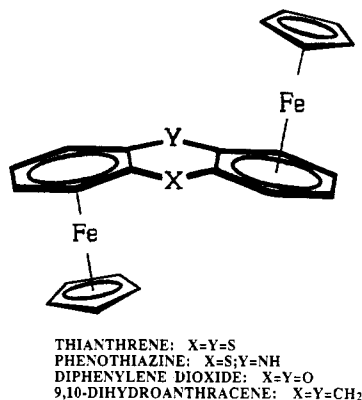
(1) Astruc, D. *Acc. Chem. Res.* **1986**, *19*, 377.

THIANTHRENE: X=Y=S
PHENOTHIAZINE: X=S;Y=NH
DIPHENYLENE DIOXIDE: X=Y=O
9,10-DIHYDROANTHRACENE: X=Y=CH₂

**Figure 1.** Structures of the $(\eta^6,\eta^6\text{-arene})\text{bis}(\eta^5\text{-cyclopentadienyliron(II)})$ dication complexes.

rocenes,[6–9] which tend to resist reduction, these complexes exhibit reversible electron transfer and produce stable reduced products at fairly negative potentials ($E^\circ$ = ca. −1.00 V vs NHE):[10–12]

$$[\text{Ar}(\text{Fe}^{\text{II}}\text{cp})]^+ + e^- \rightleftharpoons \text{Ar}(\text{Fe}^{\text{I}}\text{cp})$$
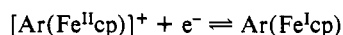
where Ar = arene, cp = cyclopentadienyl.

These stable, reduced forms can act as electron reservoirs,[1,13] catalyzing the reduction of other solution species through homogeneous charge transfer, where a kinetic overpotential barrier prevents heterogeneous charge transfer.[14] The degree of substitution of the arene ligand affects the stability of the reduced complex. Peralkylated arenes tend to impart stability to the extent that reduced, neutral complexes can be isolated quantitatively.[3] The choice of solvent affects stability as well.[15] Electron-donating solvents such as acetonitrile destabilize the reduced complex by displacing the arene ligand. While the mechanism for the reduction of the arene complexes in acetonitrile has been described qualitatively,[11] no cyclic voltammetric (CV) studies have been carried out at fast scans to determine the rate constants of the reactions. The work reported here comprises CV investigations that include fast scan rates (>1 V/s) with digital simulations to extract the rate constants for coupled homogeneous reactions.

Because of the unusual stability of these reduced complexes and the effect of substitution on the ligand, molecular orbital calculations[5] and spectroscopic studies[3,4] have been previously carried out to determine the odd-electron density profile. IND-O–SCF calculations imply that the electron added during reduction resides predominantly in a ligand-based orbital. However, extensive spectroscopic studies, including Mössbauer and ESR, reveal that the extra electron density is centered in a metal-based orbital. The antibonding orbital containing the odd electron was approximated to be 75% metal-based from Mössbauer results. The orbital also has slightly more cp than arene character in the benzene case.

Recent interest in the diiron complexes has been specifically directed at the possibility of interaction of the iron centers.[1,10] Since the odd electron is mostly metal localized, it is claimed that the metals should strongly interact in the case of a delocalized bridging ligand or should be independent in the case of a nonconjugated system. The extent of the interaction is indicated by the difference in reduction potentials of the two metal centers. Thus, cyclic voltammetry is informative in assessing the extent of metal–metal interaction.

## Experimental Section

**Chemicals.** $(\eta^6,\eta^6\text{-Arene})\text{bis}((\eta^5\text{-cyclopentadienyl})\text{iron(II)})$ dications (arene = thianthrene, diphenylene dioxide, and phenothiazine) were prepared as hexafluorophosphate salts as described previously.[16–18] Additionally, $(\eta^6\text{-thianthrene})(\eta^5\text{-cyclopentadienyl})\text{iron(II)}$ monocation was prepared by a previously described ligand-exchange reaction.[16] Tetra-*n*-butylammonium hexafluorophosphate ((TBA)PF₆), used as supporting electrolyte, was obtained from Southwestern Analytical Chemicals (Austin, TX). Prior to use, (TBA)PF₆ was twice recrystallized from ethyl acetate/ether and vacuum-dried at 110 °C for 24 h. Solvents used in electrochemical measurements included acetonitrile (MeCN) and methylene chloride (CH₂Cl₂). MeCN (MCB) was purified by stirring in contact with CaH₂, followed by distillation onto Woelm activated Al₂O₃. The dried MeCN was vacuum-distilled onto freshly activated alumina and stored in a drybox under a He atmosphere. CH₂Cl₂ (Fisher Scientific) was dried over CaH₂ and vacuum-distilled onto fresh CaH₂ for storage. Both solvents were degassed by two cycles of freeze–pump–thaw just before use.

**Measurements.** Electrochemical measurements were performed with a Princeton Applied Research (PAR) Model 175 universal programmer, a PAR Model 173 potentiostat, and a PAR Model 179 digital coulometer (Princeton Applied Research Corp., Princeton, NJ). Voltammograms were recorded on a Model 2000 X-Y recorder (Houston Instruments, Inc., Austin, TX) or a Model 7046B X-Y recorder (Hewlett-Packard Co., San Diego, CA). Electrolysis experiments were also performed on the BAS-100 electrochemical analyzer (Bioanalytical Systems, Inc., West Lafayette, IN). Data acquisition at fast scan rates (>1 V/s) was carried out with a Model 3001 processing oscilloscope (Norland Corp., Fort Atkinson, WI). The electrochemical cells were of the one- and three-compartment designs.[19] A three-electrode configuration was used, consisting of a Pt-disk working electrode (sealed in glass), a Ag-wire quasi-reference electrode, and a vitreous-carbon or Pt-gauze counter electrode. Electrochemical potentials were determined with respect to the ferrocene (Fc) couple and then reported vs NHE, with $E^\circ$ of the Fc⁺/Fc couple taken as +0.549 V vs NHE.[20] Digital simulations were performed on the UT-CDC 6000 dual cyber computer (Control Data Corp.).

## Results and Discussion

**$(\eta^6\text{-Thianthrene})(\eta^5\text{-cyclopentadienyl})\text{iron(II)}$ (1⁺).** To compare these ligand systems with the benzene system, which has been studied extensively,[3–5,11,12,21] we first investigated the monoiron cyclopentadienyl complex of thianthrene (1⁺). The monoiron complex was soluble in several solvents suitable for cathodic electrochemical studies.[22] Methylene chloride and MeCN were chosen, because they show considerable differences in their ability to displace ligands coordinated to metal centers[23] and are easy to purify. Cyclic voltammetry of 1⁺ indicates a reversible one-electron reduction in methylene chloride at a potential $E^\circ$ = −0.92 V vs NHE (Figure 2a). Although the peak splitting ($\Delta E_p = E_{pa}$

(2) Muetterties, E. L.; Bleeke, J. R.; Wucherer, E. J. *Chem. Rev.* **1982**, *82*, 499.

(3) Hamon, J.-R.; Astruc, D.; Michaud, P. *J. Am. Chem. Soc.* **1981**, *103*, 758.

(4) Rajasekharan, M. V.; Giezynski, S.; Ammeter, J. H.; Oswald, N.; Michaud, P.; Hamon, J. R.; Astruc, D. *J. Am. Chem. Soc.* **1982**, *104*, 2400.

(5) Clack, D. W.; Warren, K. D. *J. Organomet. Chem.* **1978**, *152*, C60.

(6) Moulton, R. D.; Bard, A. J. *Organometallics* **1988**, *7*, 351.

(7) Trifan, D. S.; Nicholas, L. J. *J. Am. Chem. Soc.* **1957**, *79*, 2746.

(8) Mugnier, Y.; Moise, C.; Tirouflet, J.; Laviron, E. *J. Organomet. Chem.* **1980**, *186*, C49.

(9) Ito, N.; Saji, T.; Aoyagui, S. *J. Organomet. Chem.* **1983**, *247*, 301.

(10) Lacoste, M.; Desbois, M.-H.; Astruc, D. *Nouv. J. Chim.* **1987**, *11*, 561.

(11) Darchen, A. *J. Chem. Soc., Chem. Commun.* **1983**, 768; *J. Organomet. Chem.* **1986**, *302*, 389.

(12) Moinet, C.; Roman, E.; Astruc, D. *J. Electroanal. Chem. Interfacial Electrochem.* **1981**, *121*, 241.

(13) Astruc, D. *Tetrahedron* **1983**, *39*, 4027.

(14) Buet, A.; Darchen, A.; Moinet, C. *J. Chem. Soc., Chem. Commun.* **1979**, 447.

(15) Nesmeyanov, A. N.; Vol'kenau, N. A.; Shilovtseva, L. S.; Petrokova, V. A. *J. Organomet. Chem.* **1973**, *61*, 329.

(16) Lee, C. C.; Piórko, A.; Sutherland, R. G. *J. Organomet. Chem.* **1983**, *248*, 357.

(17) Lee, C. C.; Steele, B. R.; Sutherland, R. G. *J. Organomet. Chem.* **1980**, *186*, 265.

(18) Sutherland, R. G.; Iobal, M.; Piórko, A. *J. Organomet. Chem.* **1986**, *302*, 307.

(19) Smith, W. H.; Bard, A. J. *J. Am. Chem. Soc.* **1975**, *97*, 5203.

(20) Gritzner, G.; Kuta, J. *Pure Appl. Chem.* **1982**, *5*, 1527.

(21) Vol'kenau, N. A.; Petrakova, V. A. *Abstracts of Papers*, 5th International Conference on Organometallic Chemistry, Moscow, 1971; Vol. II, No. 354.

(22) Mann, C. K. In *Electroanalytical Chemistry*; Bard, A. J., Ed.; Marcel Dekker: New York, 1969; Vol. 3, p 58.

(23) Fry, A. J.; Britton, W. E. In *Laboratory Techniques in Electroanalytical Chemistry*; Kissinger, P. T., Heineman, W. R., Eds.; Marcel Dekker: New York, 1984; p 372.

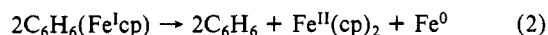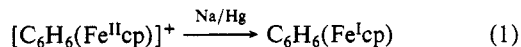**Table I.** Dependence of Peak Current Function on Scan Rate[a]

| $v$, mV/s | $E_{pc1}$, V | $i_{pc1}/v^{1/2}$ [b] | $E_{pc2}$, V | $i_{pc2}/v^{1/2}$ [c] | $i_{pci}/v^{1/2}$ [d] |
|---|---|---|---|---|---|
| 50 | 0.806 | 0.99 | 1.019 | 5.20 | 3.47, 3.37 |
| 100 | 0.830 | 1.22 | 1.039 | 4.65 | 3.50, 3.48 |
| 200 | 0.862 | 1.51 | 1.070 | 4.45 | 3.36, 3.53 |
| 500 | 0.897 | 1.77 | 1.096 | 3.73 | 3.13, 3.53 |
| 1000 | 0.924 | 2.02 | 1.114 | 3.32 | 3.42, 3.20 |

[a] Potentials vs NHE (based on $Fc^+/Fc$ as +0.549 vs NHE); $i_{pc}/v^{1/2}$ in $\mu A/mV^{1/2}$. [b] $i_{pc1}$ = cathodic peak current for reduction of $2^{2+}$ at $E_{pc1}$; MeCN, $C^*$ = 5 mM. [c] $i_{pc2}$ = cathodic peak current for reduction of $2^{2+}$ at $E_{pc2}$. [d] $i_{pci}$ = cathodic peak current for reduction of $1^+$; $C^*$ = 5 mM; in $CH_2Cl_2$, $CH_3CN$, respectively.
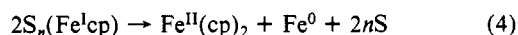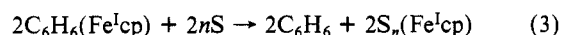
– $E_{pc}$) was 70 mV, Nernstian behavior is assumed, since the reference couple $Fc^+/Fc$ also showed a $\Delta E_p$ of 70 mV, indicating that uncompensated solution resistance was significant. The $E°$ for this couple is 150 mV positive that of $[C_6H_6(Fe^{II}cp)]^+$ ($E°$ = 1.07 V).[11] The peak current ratio ($i_{pa}/i_{pc}$) was near unity at scan rates greater than 100 mV/s. Below 100 mV/s, the ratio decreased (e.g., at 50 mV/s, $i_{pa}/i_{pc}$ = 0.76), suggesting a following chemical reaction that consumes the reduced material. From the Nicholson and Shain treatment of EC$_i$ processes,[24] we estimate the rate constant of the homogeneous chemical process to be $k$ = 0.02 s$^{-1}$, assuming a first-order chemical process.

Cyclic voltammetry of $1^+$ in MeCN (Figure 2b) shows no reoxidation of the reduced species below a scan rate of 1 V/s. This suggests that the following chemical reaction rate constant is at least 2 orders of magnitude larger in MeCN compared to that in methylene chloride.

Bulk electrolysis carried out at –1.15 V in MeCN passed an amount of charge equivalent to 1.0 electron/equiv. During reduction, a black, finely divided solid formed, which adhered to the stir bar. Subsequent cyclic voltammetry of the electrolyzed solution showed oxidations for both ferrocene and free thianthrene. The process responsible for this behavior is thus completely analogous to the reported chemical reduction of the benzene complex,[15,21] which yields benzene, ferrocene, and zerovalent iron:
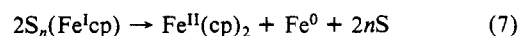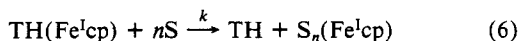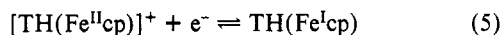
$$[C_6H_6(Fe^{II}cp)]^+ \xrightarrow{Na/Hg} C_6H_6(Fe^Icp) \quad (1)$$

$$2C_6H_6(Fe^Icp) \rightarrow 2C_6H_6 + Fe^{II}(cp)_2 + Fe^0 \quad (2)$$

The reaction in eq 2 actually involves several steps:

$$2C_6H_6(Fe^Icp) + 2nS \rightarrow 2C_6H_6 + 2S_n(Fe^Icp) \quad (3)$$

$$2S_n(Fe^Icp) \rightarrow Fe^{II}(cp)_2 + Fe^0 + 2nS \quad (4)$$

where S = solvent.

The rate constant ($k$) determined above for the reaction of reduced $1^+$ in methylene chloride probably represents the pseudo-first-order solvent displacement of the arene ligand, since $k$ is strongly dependent on choice of solvent [i.e. $k$(MeCN) $\gg$ $k$(CH$_2$Cl$_2$)]. The rate constant for the second-order disproportionation would presumably be less sensitive to solvent choice. The mechanism proposed for the reduction of the thianthrene–monoiron complex is

$$[TH(Fe^{II}cp)]^+ + e^- \rightleftharpoons TH(Fe^Icp) \quad (5)$$

$$TH(Fe^Icp) + nS \xrightarrow{k} TH + S_n(Fe^Icp) \quad (6)$$

$$2S_n(Fe^Icp) \rightarrow Fe^{II}(cp)_2 + Fe^0 + 2nS \quad (7)$$

**($\eta^6,\eta^6$-Thianthrene)bis(($\eta^5$-cyclopentadienyl)iron(II)) ($2^{2+}$).** Since this complex is insoluble in methylene chloride and other noncoordinating solvents, the different solvent effects for $1^+$ compared to $2^{2+}$ could not be addressed. Instead, we compare the electrochemical behavior of $1^+$ and $2^{2+}$ in MeCN. Cyclic voltammetry of $2^{2+}$ over the same range of scan rates shows two reductions, but no coupled oxidations (Figure 3), with peak potentials of $E_{pc1}$ = –0.81 V and $E_{pc2}$ = –1.02 V vs NHE (at $v$ =
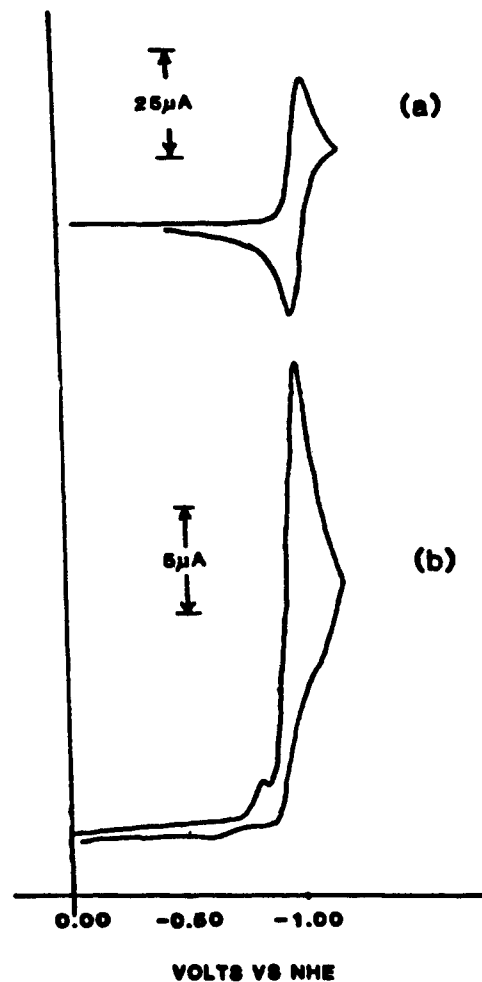
(24) Nicholson, R. S.; Shain, I. *Anal. Chem.* **1964**, *36*, 706.



**Figure 2.** Cyclic voltammetry at a Pt electrode of 5 mM $1^+$ in (a) 0.1 M (TBA)PF$_6$, CH$_2$Cl$_2$, at $v$ = 200 mV/s and (b) 0.1 M (TBA)PF$_6$, CH$_3$CN, at $v$ = 200 mV/s. The prewave in (b) is due to an adsorbed species. Polishing of the electrode eliminated this peak.
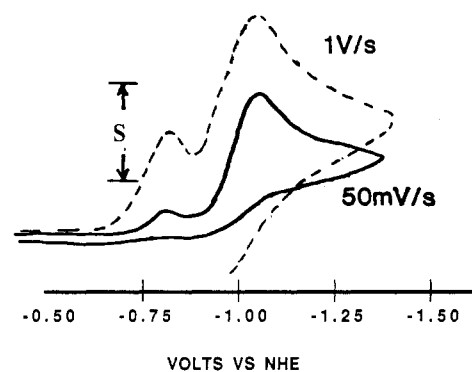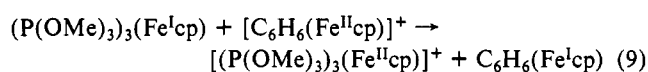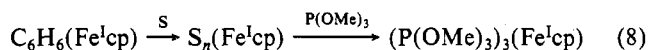


**Figure 3.** Cyclic voltammetry of 5 mM $2^{2+}$ in 0.1 M (TBA)PF$_6$, CH$_3$CN: (a) solid line, $v$ = 50 mV/s ($s$ = 10 $\mu$A); (b) dashed line, $v$ = 1 V/s ($s$ = 25 $\mu$A).

50 mV/s). Table I shows the peak currents ($i_{pc}$) normalized by the square root of the scan rate ($v^{1/2}$) for the reductions of $2^{2+}$ in MeCN. In the case of a one-electron reversible reduction unperturbed by coupled homogeneous reactions, the peak current function ($i_{pc}/v^{1/2}$) is constant at all scan rates. The peak current function for the reduction of $1^+$ ($i_{pci}$) in methylene chloride, also shown in Table I, conforms quite well to this behavior.

Both current functions for $2^{2+}$ show different behavior over this scan rate range. As $v$ increases, $i_{pc1}/v^{1/2}$ increases while $i_{pc2}/v^{1/2}$ decreases. To show that the effects were not simply due to the coupled solvent displacement reaction observed in MeCN for the monoiron complex, the peak current function for $1^+$ in MeCN was calculated and shown to be constant over the same scan rate
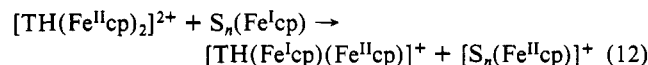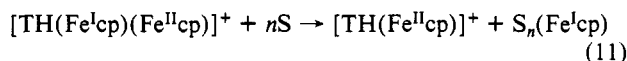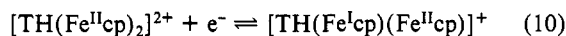
range. These findings imply that other coupled homogeneous reactions are responsible for the deviations in the current functions for $2^+$.

The $i_{pc1}/v^{1/2}$ behavior suggests that a chemical process that consumes the parent material ($2^{2+}$) occurs at a rate that is fast compared to the time scale characteristic of the CV scan rate. A similar process has been described for the bulk reduction of the benzene complex. Darchen observed that only catalytic amounts of current (i.e., $n \ll 1$ when calculated from the amount of charge passed) were required to reduce the compound $[(C_6H_6)Fe^{II}cp]^+$ in MeCN in the presence of $P(OMe)_3$.[11] He proposed that ultimately 3 equiv of $P(OMe)_3$ displaced the benzene ligand from the reduced benzene–iron complex. The ($P(OMe)_3)_3(Fe^Icp)$ species is a powerful enough reducing agent to reduce an equivalent of parent material. The mechanism is thus reaction 1 followed by

$$C_6H_6(Fe^Icp) \xrightarrow{S} S_n(Fe^Icp) \xrightarrow{P(OMe)_3} (P(OMe)_3)_3(Fe^Icp) \quad (8)$$

$$(P(OMe)_3)_3(Fe^Icp) + [C_6H_6(Fe^{II}cp)]^+ \rightarrow$$
$$[(P(OMe)_3)_3(Fe^{II}cp)]^+ + C_6H_6(Fe^Icp) \quad (9)$$

The overall net reaction is thus a ligand replacement reaction with conversion of $[C_6H_6(Fe^{II}cp)]^+$ to $[(P(OMe)_3)_3Fe^{II}cp]^+$, with only a small amount of current needed to generate $C_6H_6(Fe^Icp)$ initially. The rate-limiting step, however, was believed to be the formation of the solvent-complexed intermediate ($C_6H_6$–$Fe^Icp \rightarrow$ $S_n$–$Fe^Icp \rightarrow$ ($P(OMe)_3)_3$–$Fe^Icp$), consistent with the chemical reduction mechanism shown in reactions 3 and 4.

For the thianthrene complex, $2^{2+}$, we propose that the iron-(I)–solvent complex reduces the starting material directly, so that the proposed mechanism for the voltammetry observed at $E_{pc1}$ is

$$[TH(Fe^{II}cp)_2]^{2+} + e^- \rightleftharpoons [TH(Fe^Icp)(Fe^{II}cp)]^+ \quad (10)$$

$$[TH(Fe^Icp)(Fe^{II}cp)]^+ + nS \rightarrow [TH(Fe^{II}cp)]^+ + S_n(Fe^Icp) \quad (11)$$

$$[TH(Fe^{II}cp)_2]^{2+} + S_n(Fe^Icp) \rightarrow$$
$$[TH(Fe^Icp)(Fe^{II}cp)]^+ + [S_n(Fe^{II}cp)]^+ \quad (12)$$

While the species $S_n(Fe^Icp)$ may not be as strong a reducing agent as the $P(OMe)_3$ complex, the ease with which $2^{2+}$ is reduced relative to other arene complexes makes the homogeneous charge transfer (12) much easier thermodynamically. The process responsible for the behavior of $i_{pc2}/v^{1/2}$ is not clearly determined at the slow scan rates imposed. Since the peak potential ($E_{pc2}$) is coincident with the peak potential for the reduction of $1^+$, the monoiron species formed in eq 11 is obviously contributing to the second current function ($i_{pc2}/v^{1/2}$) for $2^{2+}$. The fact that the current function decreases with increasing $v$ supports this hypothesis, since the amount of $1^+$ generated depends on $k_{11}$, the rate constant for eq 11. If $k_{11}$ is sufficiently slow, increasing $v$ will diminish the concentration of $1^+$ at the electrode and therefore decrease $i_{pc2}/v^{1/2}$. We show below by studies at high $v$ that $2^{2+}$ is reduced directly in a two-electron reaction near $E_{pc2}$ before decomplexation occurs.

The observed current functions suggest that $k_{11}$ is no more than 1 or 2 orders of magnitude greater than the characteristic CV time scale. If $k_{11}$ was very large, $i_{pc1}/v^{1/2}$ would be near zero (assuming that the homogeneous charge-transfer reaction (12) is fast), with conversion of $[TH(Fe^{II}cp)_2]^{2+}$ to $[TH(Fe^{II}cp)]^+$ and $[S_n(Fe^{II}cp)]^+$ after initial generation of only a small amount of reduced species, $2^+$. At the second peak, $i_{pc2}/v^{1/2}$ would approach that for a simple 1e reduction of $[TH(Fe^{II}cp)]^+$. By application of faster scan rates, two uncertainties can be resolved: (1) the exact value of $k_{11}$ and (2) whether $i_{pc2}/v^{1/2}$ will decay to zero as $k_{11}$ is overwhelmed by $v$. If, however, $i_{pc2}/v^{1/2}$ approaches unperturbed 1e behavior at fast scans, then it can be deduced that $2^{2+}$ is reduced at $E_{pc2}$ to $2^+$ and then to 2, in two successive and rapid steps.

To diminish the effect of solution resistance over a wide range of scan rates, a 25-$\mu$m-diameter Pt ultramicroelectrode was used for fast scans.[25] The reduction of $2^{2+}$ at a scan rate of 20 V/s
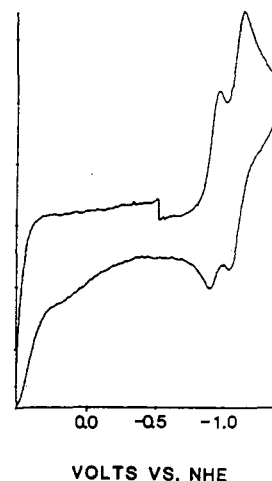


**VOLTS VS. NHE**

**Figure 4.** Cyclic voltammetry of 3 mM $2^{2+}$ in 0.1 M $(TBA)PF_6$, $CH_3$-CN, at $v = 20$ V/s.
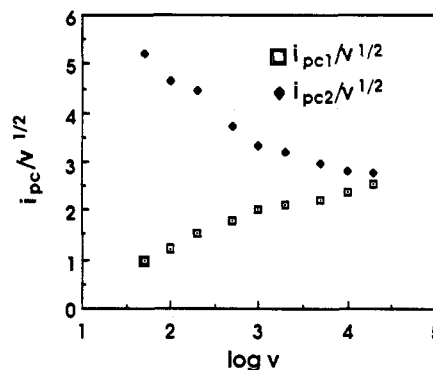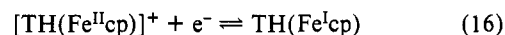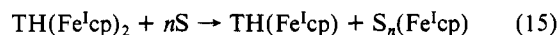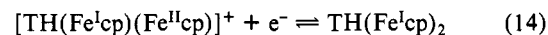


**Figure 5.** $i_{pc}/v^{1/2}$ vs log $v$ with $i_{pc}$ in $\mu_A$ and $v$ in mV/s. The peak current data at fast scans ($>1$ V/s), obtained with an ultramicroelectrode, were adjusted to account for the differences in the areas of the electrodes and concentrations.

(Figure 4) shows two reduction waves with coupled reoxidations on scan reversal, indicating stepwise reduction of $2^{2+}$, presumably at each iron center, with $E^\circ_1 = -0.82$ V and $E^\circ_2 = -1.00$ V. A plot of $i_p/v^{1/2}$ values for both steps as a function of $v$ is shown in Figure 5. Note that at faster scan rates, the current functions of both processes converge to the same value, corresponding to the 1e value found with the monoiron species. The heterogeneous kinetics of each reduction differed at scan rates greater than 10 V/s. At 20 V/s, $\Delta E_p$ for the first reduction process is 74 mV, while $\Delta E_p$ for the second process is 105 mV, suggesting the second electron transfer is slower.

Since $2^{2+}$ is clearly being reduced in a second step at the second reduction potential and the product will probably undergo the same solvent displacement reaction described above at the slow scan rates, the following mechanism is proposed for the process at the second reduction peak:

$$[TH(Fe^{II}cp)_2]^{2+} + e^- \rightleftharpoons [TH(Fe^Icp)(Fe^{II}cp)]^+ \quad (13)$$

$$[TH(Fe^Icp)(Fe^{II}cp)]^+ + e^- \rightleftharpoons TH(Fe^Icp)_2 \quad (14)$$

$$TH(Fe^Icp)_2 + nS \rightarrow TH(Fe^Icp) + S_n(Fe^Icp) \quad (15)$$

$$[TH(Fe^{II}cp)]^+ + e^- \rightleftharpoons TH(Fe^Icp) \quad (16)$$

$$TH(Fe^Icp) + nS \rightarrow TH + S_n(Fe^Icp) \quad (17)$$
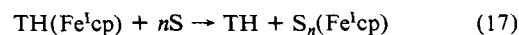
Note that $[TH(Fe^{II}cp)]^+$ in eq 16 arises from the reaction in eq 11, where the monoiron species is produced by the decomplexation of an iron(I)–cp moiety when $2^{2+}$ is reduced. The reduction of $1^+$ in MeCN was also probed at an ultramicroelectrode at faster scan rates to determine the value of $k$. At 2 V/s,

(25) Bond, A. M.; Fleischmann, M.; Robinson, J. *J. Electroanal. Chem. Interfacial Electrochem.* **1984**, *168*, 299.

the peak current ratio, $i_{pa}/i_{pc}$, was 0.55. This suggests a value of $k = 6.2$ s$^{-1}$ for the solvent displacement reaction.

If one considers eq 11, 14, and 16, there would seem to be a conservation of reducible material at the electrode for the second reduction process. Specifically, the amount of $2^+$ lost to decomplexation in eq 11 is gained back by the formation of $1^+$; since $1^+$ and $2^+$ are reduced at about the same potential, their individual reductions would be indistinguishable. Since the current function for the second wave increases with decreasing scan rate, other factors must be considered.

One possible factor is the difference in diffusion coefficients for $1^+$ and $2^{2+}$ (presumably, $D$ for $1^+$ is greater than that for $2^{2+}$). This would lead to the effect seen at slow scan rates, since more $1^+$ is produced in the vicinity of the electrode. The difference in diffusion coefficients can be determined by CV measurements with equal concentrations of $2^{2+}$ and $1^+$ at fast scans. The peak current $i_{pc2}$ in the mixture was approximately 10% larger than that predicted for an equimolar mixture with equal diffusion coefficients for both species. Another possible contributing factor is that the following reactions (eq 15 and 17) increase the current function. This effect of an irreversible following reaction is well-known and has been described theoretically,[26] but typically increases the current function by only about 5%.

**Digital Simulations.** To verify the mechanism proposed, as well as to determine the rate constants for reactions 11, 15, and 17 ($k_{11}$, $k_{15}$, $k_{17}$, respectively), we undertook digital simulations of the cyclic voltammetric behavior. Digital simulation also provides the rate constant for the homogeneous charge transfer (eq 12, $k_{12}$), which is otherwise difficult to estimate directly from the CV behavior.

Simulation of this mechanism (eq 10–17), which includes three heterogeneous charge transfers and four coupled homogeneous reactions, could be carried out by the usual methods[27] but is complicated when previous program designs are used. With three heterogeneous charge transfers, the appropriate finite difference equations are difficult to derive. The difficulty arises from the practice of expressing one flux element purely in terms of known concentrations and heterogeneous rates. Extensive algebraic manipulations are required to separate any one flux element from the others when coupled charge transfers are considered.[28] In fact, mechanisms involving only two coupled charge transfers require protracted mathematical treatment.[29] An alternative approach to solving the flux equations is to set up a heterogeneous rate constant matrix and to solve the matrix by Gaussian elimination[30] with respect to species' concentrations at the electrode surface. A description of the procedure is contained in the Appendix, and further details and a documented program are given elsewhere.[31] Briefly, a solution matrix is prepared that contains the values of the flux elements for the solution species. Homogeneous reaction effects and diffusion are modeled as described by Feldberg.[27]

From the Nicholson and Shain[24] treatment and the fact that reversibility becomes apparent at 5 V/s, the value for $k_{11}$ is estimated as approximately 10 s$^{-1}$. The use of this value for $k_{11}$ in the simulation requires that the second-order homogeneous rate, $k_{12}$, be approximately $10^5$ M$^{-1}$ s$^{-1}$ to achieve good agreement between simulated and experimental cyclic voltammograms (Figure 6). The value of the second decomplexation rate constant
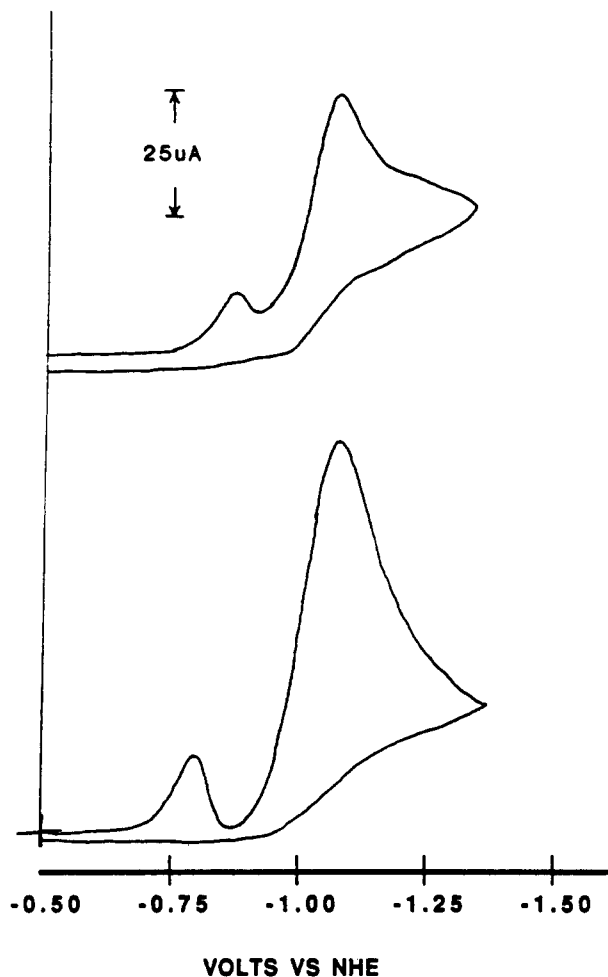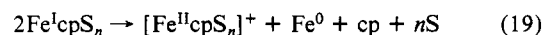
(26) Bard, A. J.; Faulkner, L. R. *Electrochemical Methods*; John Wiley and Sons: New York, 1980; p 452.
(27) Feldberg, S. W. Digital Simulation: A General Method For Solving Electrochemical Diffusion-Kinetics Problems. In *Electroanalytical Chemistry*; Bard, A. J., Ed.; Marcel Dekker: New York, 1969; Vol. 3, Chapter 4.
(28) Feldberg, S. W. Digital Simulation of Electrochemical Surface Boundary Phenomena: Multiple Electron Transfer and Absorption. In *Computers in Electrochemistry and Instrumentation*; Mattson, J. S., Mark, H. B., McDonald, H. C., Jr., Eds.; Marcel Dekker: New York, 1972; Vol. 2, p 185.
(29) Gaudiello, J. G.; Wright, T. C.; Jones, R. A.; Bard, A. J. *J. Am. Chem. Soc.* **1985**, *107*, 888.
(30) Kreyszig, E. *Advanced Engineering Mathematics*; John Wiley and Sons: New York, 1962; p 431.
(31) Bligh, R. Q. M. A. Thesis, The University of Texas at Austin, 1988.



**VOLTS VS NHE**

**Figure 6.** (a, Top) Experimental voltammogram and (b, bottom) simulated voltammogram ($k_{11} = 10$ s$^{-1}$; $k_{12} = 1.5 \times 10^5$ M$^{-1}$ s$^{-1}$; $k_{15} = 8$ s$^{-1}$; $k_{17} = 6$ s$^{-1}$) of $2^{2+}$, $\nu = 100$ mV/s.

($k_{15}$) for $2^{2+}$ was estimated from the variation of $i_{pc2}$ with scan rate studies and confirmed by digital simulation. Both provided a value of 8 s$^{-1}$ for $k_{15}$. This is about the same (within experimental error) as the decomplexation rate determined for the monoiron species that is reduced at the same potential, where $k_{17}$ is 6 s$^{-1}$.

Although good qualitative agreement was shown between the simulated and experimental voltammograms, the fit was not quantitatively correct. The actual decay of $i_{pc1}$ as the potential is scanned negatively is more gradual than that seen in the simulation (see Figure 6). This additional current between $i_{pc1}$ and $i_{pc2}$ may be due to a species produced in another reaction for which no model charge-transfer variable has been included in the simulation. One possibility is the direct reduction of the iron(II)–cp–solvent species generated in eq 12. This leads to an additional heterogeneous charge-transfer reaction in the simulation:

$$[Fe^{II}cpS_n]^+ + e^- \rightleftharpoons Fe^IcpS_n \qquad (18)$$

The potential at which this reduction occurs probably lies between $E°_1$ and $E°_2$. This restriction is applied because the reduced iron–cp–solvent species is apparently incapable of reducing either $1^+$ or $2^+$ in the same way that it reduces $2^{2+}$. The potential was arbitrarily set to $E°_1$. We also included another homogeneous electron-transfer equation to account for the probable disproportionation of the iron(I)–cp–solvent species:

$$2Fe^IcpS_n \rightarrow [Fe^{II}cpS_n]^+ + Fe^0 + cp + nS \qquad (19)$$

The addition of eq 18 and 19 results in better agreement between experiment and simulation (Figure 7). To obtain a satisfactory fit, the heterogeneous rate constant for the reduction of iron(II)–cp–solvent was such that the reaction in eq 18 was nearly irreversible ($k_{18} < 10^{-3}$ cm/s and $\alpha = 0.7$). The inclusion
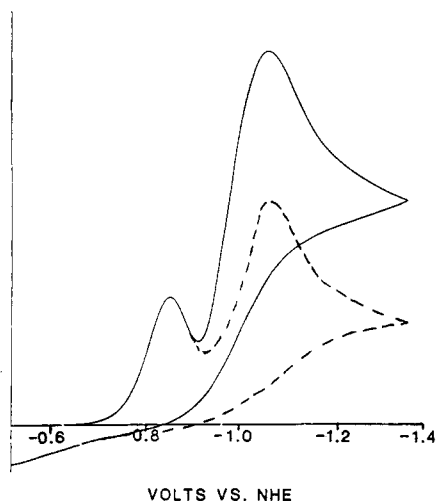
**Figure 7.** Simulated voltammogram of $2^{2+}$ at $v = 100$ mV/s, with additional heterogeneous (eq 18; $k_{18} = 5 \times 10^{-4}$) and homogeneous (eq 19; $k_{19} = 100$ M$^{-1}$ s$^{-1}$) reactions. The dashed line represents the contribution of $2^{2+}$ alone to the current function (i.e., $k_{16} = 0$).

of eq 18 and 19 in the simulation led to an $i_{pc2}$ value that was increased relative to $i_{pc1}$ (compared to earlier simulations) due to overlap of the broad peak arising from the reduction of iron-(II)–cp–solvent species (eq 18). This finding provides another explanation for the positive deviation of $i_{pc2}$ from ideal behavior at slow scan rates. In fact, the reduction of the iron(II)–cp–solvent species is probably the main factor that causes an increase in $i_{pc2}$ at slow scan rates.

Digital simulation also allows the determination of the relative contributions of $1^+$ and $2^{2+}$ to the second current function. To illustrate this, the charge-transfer rate for the reduction of $1^+$ (eq 16) was set to zero. The difference between the solid line and the dashed line in Figure 7 thus shows the importance of the contribution of $1^+$ to the overall current observed at $i_{pc2}$ for $v = 200$ mV/s.

**Effect of Addition of Carbon Monoxide.** CO was added to a solution of $2^{2+}$ to determine if the effect of the homogeneous charge transfer, eq 12, on the voltammetric response could be altered. CO is a better $\pi$-acceptor than MeCN. If CO, rather than MeCN, reacts with $2^+$ in eq 11, or displaced MeCN, the CO–iron(I) complex might not transfer an electron to the parent compound. The general reaction proposed for the CO displacement of the solvent is

$$S_n(Fe^Icp) + xCO \rightarrow (CO)_xS_{n-x}(Fe^Icp) \qquad (20)$$

Cyclic voltammetry of $2^{2+}$ with the solution saturated with CO (Figure 8a) clearly shows this inhibitory effect. Even at 50 mV/s, the relative sizes of $i_{pc1}$ and $i_{pc2}$ are equal, suggesting that no parent material is being consumed by reaction 12. IR spectroscopy gives strong evidence that reaction 20 occurs. A CO stretch at about 1990 cm$^{-1}$ indicative of carbonyl bound to iron(II)–cp half-sandwich dimers[32] was observed following bulk electrolysis of $2^{2+}$ at $-1.25$ V, suggesting that the product of reaction 20 reacts further. As observed for cases in absence of homogeneous reaction complications, the current function $i_{pc1}/v^{1/2}$ in the presence of CO was constant at all scan rates down to 50 mV/s. Digital simulation of the effect of adding CO can be demonstrated by setting $k_{12}$ to zero, as illustrated in Figure 8b.

**Comparative CV Studies of Similar Heterocyclic Ligands.** In addition to the thianthrene complex, the CV behavior of the diiron complexes of phenothiazine, diphenylene dioxide, and 9,10-dihydroanthracene in MeCN was investigated at fast scan rates at an ultramicroelectrode. These complexes, which are all anthracene analogues, will have nearly the same metal–metal distances. This simplifies the intercomplex comparisons, so that we need only consider the effects of the differences in geometry and heteroatoms
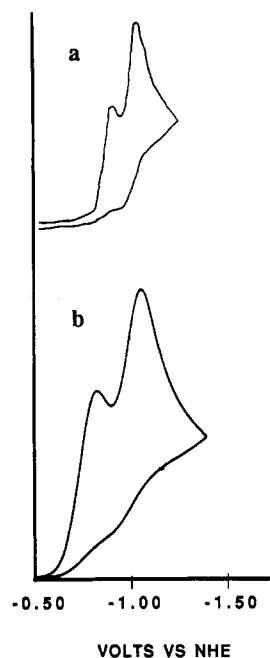


**Figure 8.** (a) Experimental voltammogram of 5 mM $2^{2+}$ at $v = 100$ mV/s, with solution saturated with CO. (b) Simulated voltammogram of $2^{2+}$ at $v = 100$ mV/s; no second-order reaction (i.e., $k_{12} = 0$).

**Table II.** Dependence of $\Delta E^\circ$ on the Dihedral Angle of the Heterocyclic Ligand

| ligand | dihedral angle,[41–44] deg | $\Delta E^\circ$, mV |
|---|---|---|
| thianthrene | 128 | 180 |
| phenothiazine | 153 | 125 |
| diphenylene dioxide | 180 | 219 |
| 9,10-dihydroanthracene | 160 | 125 |
| 9,10-dihydroanthracene[10] | 160 | 100 |
| diphenylmethane[10] | 180 | 90 |
| p-terphenyl[10] | 180 | 80 |
| phenanthrene[10] | 180 | 180 |
| 9,10-dihydrophenanthrene[10] | 180 | 160 |

in the different compounds on the CV behavior.

At a scan rate of 60 V/s, all the systems show two reversible 1e waves, as was seen with the thianthrene complex at large $v$. The values for $\Delta E^\circ$ (the difference in potential between the first and second reduction steps) were measured for these complexes and are given in Table II, along with dihedral angles of the unsubstituted ligands and $\Delta E^\circ$ values for similar complexes reported elsewhere.[10] The $\Delta E^\circ$ measured for 9,10-dihydroanthracene in MeCN (125 mV) is greater than that reported in DMF (100 mV), which indicates a solvation energy effect on $\Delta E^\circ$. While DMF and MeCN have virtually the same dielectric constants,[33] DMF is a superior electron donor in the solvation of cations.[34] This suggests that DMF will stabilize the dication form of the complex (i.e., promote a negative shift in $E^\circ_1$) to a greater degree than MeCN. The difference between the solvents in the stabilization of the monocation will not be as dramatic, since a smaller charge is being solvated. The net result is that the reduction potentials will be closer together in DMF than in MeCN, as observed. The effect of differences in solvation energies on the $\Delta E^\circ$ of stepwise electron transfers has been discussed previously.[35,36]

If the two iron centers in each of these complexes were completely noninteracting, we would expect the reduction potentials to be separated only by a difference caused by probability factors[37]

(32) Manning, A. R. *J. Chem. Soc* A **1968**, 1319.

(33) *Lange's Handbook of Chemistry*, 12th ed.; John A. Dean, Ed.; 1979; pp 10–109.

(34) Szwarc, M. Concept of Ion Pairs. In *Ion and Ion Pairs in Organic Reactions*; Szwarc, M., Ed.; 1972; p 1.

(35) Phelps, J.; Bard, A. J. *J. Electroanal. Chem. Interfacial Electrochem.* **1976**, *68*, 313–335.

(36) Ammar, F.; Saveant, J. M. *J. Electroanal. Chem. Interfacial Electrochem.* **1973**, *47*, 115.

in the stepwise reduction of the iron centers ($E_{pc1} - E_{pc2} = 35.6$ mV for a two-center molecule).[38] The shape of the voltammogram in the noninteracting case would be identical with a one-electron CV reduction wave. We observe that the two reduction potentials are more widely separated ($\geq 100$ mV). Thus, the Fe atoms do interact; i.e., the reduction potential of the $Fe^{II}cp$ moiety depends on the charge on the other Fe atom.

Since we observed that $\Delta E^{\circ}$ is significant in every case, we conclude that some metal–metal interaction exists for each complex. This interaction could occur through space or via delocalization through the ligand. We can attempt to correlate the interaction with the dihedral angles of the ligands. Note however, that significant geometry changes in the ligand can occur upon complex action; see, for example, X-ray structural results for related compounds with x = O, y = S and x = O, y = $CH_2$.[39] Presumably, 9,10-dihydroanthracene would represent minimum interaction for a process in which interaction depends on ligand delocalization of the electron density introduced by reduction. The nonplanarity of the ligand places the bridging $sp^3$ carbons in a suboptimal geometry for an efficient $\pi$-delocalization process. The $\Delta E^{\circ}$ value (125 mV) is a result of a combination of factors, including through-space interaction, induction, and hyperconjugation effects. In fact, the anthracene ligands with the saturated ortho bridging units are analogous to the series of compounds having two anthracene molecules joined by a methylene chain, previously examined.[40] In this case, with two intervening methylene units, the difference in the reduction potential of the two anthracene units was 100 mV in MeCN. The phenothiazine complex, with a dihedral angle close to that of 9,10-dihydroanthracene, also exhibits a $\Delta E^{\circ}$ value consistent with an interaction effect.

The $\Delta E^{\circ}$ values measured for thianthrene and diphenylene dioxide, however, seem to indicate that additional interaction through the ligand occurs. In the case of diphenylene dioxide the ligand is probably more planar than in the preceding cases, allowing for better electronic $\pi$-delocalization. While thianthrene is nonplanar, the sulfur heteroatoms, unlike nitrogen, carbon, and oxygen, have d orbitals available for $\pi$-delocalization in nonplanar geometries. The higher $\Delta E^{\circ}$ values for the nonplanar thianthrene ligand and the more planar diphenylene dioxide ligand are thus probably due to a combination of through-space interaction and increased ligand participation in the delocalization of added electron density.

## Conclusions

Elucidation of the mechanism of the electrochemical reduction of ($2^{2+}$) from experimental and simulated data confirmed prior investigations regarding the catalytic reduction of starting material by the decomplexed iron(I)–cp–solvent species. We also observed that the reduction of $2^+$ occurred at the same potential as that of $1^+$. For comparison, a previous study[10] investigated the coincidence of the reduction potential of a monoiron diphenyl species and the second reduction potential of the analogous diiron species. It was proposed that the diiron species loses an iron–cp moiety, giving rise to the monoiron species. In effect, the second reduction process for the diiron species is actually the reduction of the monoiron product. We observed this same effect for the thianthrene complex at slow scan rates. However, we also showed that at fast scan rates we observe two reversible, one-electron

(37) Flanagan, J. B.; Margel, S.; Bard, A. J.; Anson, F. C. *J. Am. Chem. Soc.* **1978**, *100*, 4248.
(38) Ammar, F.; Saveant, J. M. *J. Electroanal. Chem. Interfacial Electrochem.* **1973**, *47*, 215.
(39) (a) Lynch, V. M.; Thomas, S. N.; Simonsen, S. H.; Piórko, A.; Sutherland, R. G. *Acta Crystallogr.* **1980**, *C42*, 1144. (b) Simonsen, S. H.; Lynch, V. M.; Sutherland, R. G.; Piórko, A. *J. Organomet. Chem.* **1985**, *290*, 387.
(40) Itaya, K.; Bard, A. J.; Szwarc, M. *Z. Phys. Chem. (Munich)* **1978**, *112*, 1.
(41) Rowe, I.; Post, B. *Acta Crystallogr.* **1958**, *11*, 372.
(42) Blount, J. F.; Briscoe, O. V.; Freeman, H. C. *Chem. Commun.* **1968**, 1656.
(43) Sygula, A.; Holak, T. A. *Tetrahedron Lett.* **1983**, *24*, 2893.
(44) Kamiya, M. *Bull. Chem. Soc. Jpn.* **1972**, *45*, 1589.
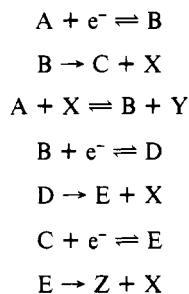
reductions of the diiron compound.

We propose that the rather large peak splitting ($\Delta E^{\circ} \approx 100$ mV) that is observed for the complexes where metal–metal interaction by electronic delocalization through the ligand is minimal is due to through-space interaction. As the metal–metal distance is increased by increasing the alkyl chain between the complexed arene rings, the peak splitting vanishes. We also observed that if the geometry of the ligand was suitable for optimal p-orbital overlap (or d-orbital, in the case of sulfur) between the heteroatoms and the arene rings, the peak splitting between the reduction of the two metal centers increased, indicating interaction through the diaryl ligand.

The utility of expressing the interdependent flux equations in a matrix form for simulation purposes has been directly and indirectly implied. As mentioned, more than two coupled heterogeneous charge transfers are very difficult to model by standard methods. Once a mechanism is proposed and modeled, it can be extremely difficult to incorporate a new heterogeneous rate parameter when necessary (as was done in this study) if the flux equations are derived by the usual algebraic manipulations. Current work involves extending the matrix method to arrive at a completely general program for simulating cyclic voltammetry.

## Appendix. Development of a General Method for Heterogeneous Charge Transfer

Before developing a general solution for the digital simulation of the heterogeneous charge-transfer process, it is informative to reconsider the flux equations for a simple, two component system:

$$A + e^- \rightleftharpoons B$$
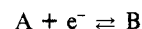
To model the flux of electroactive material at the electrode surface ($x = 0$), we define the fluxes in both rigorous and finite difference forms:

$$f_A = k_{fAB}C_A(0) - k_{bAB}C_B(0) \tag{A1}$$

$$f_A = D_A(\Delta C_A/\Delta x)_{x=0} = 2D_A/\Delta x[C_A(1) - C_A(0)] \tag{A2}$$

$$f_B = k_{bAB}C_B(0) - k_{fAB}C_A(0) \tag{A3}$$

$$f_B = D_B(\Delta C_B/\Delta x)_{x=0} = 2D_B/\Delta x[C_B(1) - C_B(0)] \tag{A4}$$

where $f_A$ = flux of species A; $k_{fAB}$ = forward heterogeneous rate for the couple A/B, $k_{bAB}$ = backward heterogeneous rate for the couple A/B, $C_A(x)$ = concentration of species A in volume element $x$, $D_A$ = diffusion coefficient of species A, and $\Delta x$ = width of each volume element. Similar definitions hold for species B.

By rearrangement of the finite difference flux equations, (A2) and (A4), we can solve for $C_A(0)$ and $C_B(0)$:

$$C_A(0) = C_A(1) - f_A\Delta x/2D_A \tag{A5}$$

$$C_B(0) = C_B(1) - f_B\Delta x/2D_B \tag{A6}$$

Substituting expressions A5 and A6 into the rigorous flux expressions, (A1) and (A3), we obtain

$$f_A = k_{fAB}[C_A(1) - f_A\Delta x/2D_A] - k_{bAB}[C_B(1) - f_B\Delta x/2D_B] \tag{A7}$$

$$f_B = k_{bAB}[C_B(1) - f_B\Delta x/2D_B] - k_{fAB}[C_A(1) - f_A\Delta x/2D_A] \tag{A8}$$

For this two-component case, eq A1 and A3 suggest that $f_B = f_A$. By substitution for $f_B$ into eq A7, $f_A$ can be determined explicitly and, subsequently, the current.

Rather than solving the flux of A by direct substitution, we can recast eq A7 and A8, collecting concentration terms on one side and flux terms on the other:

$$[1 + k_f\Delta x/2D_A]f_A + [-k_b\Delta x/2D_B]f_B = k_fC_A(1) - k_bC_B(1) \tag{A9}$$

$$[-k_f\Delta x/2D_A]f_A + [1 + k_b\Delta x/2D_B]f_B = k_bC_B(1) - k_fC_A(1) \tag{A10}$$

Equations A9 and A10 can be readily cast into the matrix formula [a] × [b] = [c], where [a] is the 2 × 2 matrix containing the coefficients of the fluxes, [b] is the 1 × 2 matrix containing the fluxes, and [c] is the 1 × 2 matrix containing the concentration terms. The solution for matrix [b] could then be found by Gaussian elimination. The advantage of this method becomes apparent when one considers the multicomponent thianthrene diiron system.

The reaction mechanism proposed for the thianthrene diiron complexes comprises eq 10–16 and can be cast in general as

$$A + e^- \rightleftharpoons B$$

$$B \rightarrow C + X$$

$$A + X \rightleftharpoons B + Y$$

$$B + e^- \rightleftharpoons D$$

$$D \rightarrow E + X$$

$$C + e^- \rightleftharpoons E$$

$$E \rightarrow Z + X$$

By analogous derivation, we can write expressions similar to those above in eq A7 and A8 for the electroactive species:

$$f_A = k_{fAB}[C_A(1) - f_A\Delta x/2D_A] - k_{bAB}[C_B(1) - f_B\Delta x/2D_B] \quad (A11)$$

$$f_B = k_{bAB}[C_B(1) - f_B\Delta x/2D_B] - k_{fAB}[C_A(1) - f_A\Delta x/2D_A] + k_{fBD}[C_B(1) - f_B\Delta x/2D_B] - k_{bBD}[C_D(1) - f_D\Delta x/2D_D] \quad (A12)$$

$$f_C = k_{fCE}[C_C(1) - f_C\Delta x/2D_C] - k_{bCE}[C_E(1) - f_E\Delta x/2D_E] \quad (A13)$$

$$f_D = k_{bBD}[C_D(1) - f_D\Delta x/2D_D] - k_{fBD}[C_B(1) - f_B\Delta x/2D_B] \quad (A14)$$

$$f_E = k_{bCE}[C_E(1) - f_E\Delta x/2D_E] - k_{fCE}[C_C(1) - f_C\Delta x/2D_C] \quad (A15)$$

Once again, we rearrange these expressions, separating concentration terms and flux terms:

$$[1 + k_{fAB}\Delta x/2D_A]f_a + [-k_{bAB}\Delta x/2D_B]f_B = k_{fAB}C_A(1) - k_{bAB}C_B(1) \quad (A16)$$

$$[1 + k_{bAB}\Delta x/2D_B + k_{fBF}\Delta x/2D_B]f_B + [-k_{fAB}\Delta x/2D_A]f_A + [-k_{bBD}\Delta x/2D_D]f_D = k_{bAB}C_B(1) - k_{fAB}C_A(1) + k_{fBD}C_B(1) - k_{bBD}C_D(1) \quad (A17)$$

$$[1 + k_{fCE}\Delta x/2D_C]f_C + [-k_{bCE}\Delta x/2D_E]f_E = k_{fCE}C_C(1) - k_{bCE}C_E(1) \quad (A18)$$

$$[1 + k_{bBD}\Delta x/2D_D]f_D + [-k_{fBD}\Delta x/2D_B]f_B = k_{bBD}C_D(1) - k_{fBD}C_B(1) \quad (A19)$$

$$[1 + k_{bCE}\Delta x/2D_E]f_E + [-k_{fCE}\Delta x/2D_C]f_C = k_{bCE}C_E(1) - k_{fCE}C_C(1) \quad (A20)$$

Finally, a matrix can be set up directly from eq A16–A20 that enables one to solve for $f_A$, $f_B$, $f_C$, $f_D$, and $f_E$:

| [a] | | | | | x | [b] = | [c] |
|---|---|---|---|---|---|---|---|
| $1 + \frac{k_{fAB}\Delta x}{2D_A}$ | $-\frac{k_{bAB}\Delta x}{2D_B}$ | 0 | 0 | 0 | | $f_A$ | $k_{fAB}C_A(1) - k_{bAB}C_B(1)$ |
| $-\frac{k_{fAB}\Delta x}{2D_A}$ | $1 + \frac{k_{bAB}\Delta x}{2D_B} + \frac{k_{fBD}\Delta x}{2D_B}$ | 0 | $-\frac{k_{bBD}\Delta x}{2D_D}$ | 0 | | $f_B$ | $k_{bAB}C_B(1) - k_{fAB}C_A(1)$ $k_{fBD}C_B(1) - k_{bBD}C_D(1)$ |
| 0 | 0 | $1 + \frac{k_{fCE}\Delta x}{2D_C}$ | 0 | $-\frac{k_{bCE}\Delta x}{2D_E}$ | | $f_C$ | $k_{fCE}C_C(1) - k_{bCE}C_E(1)$ |
| 0 | $-\frac{k_{fBD}\Delta x}{2D_B}$ | 0 | $1 + \frac{k_{bBD}\Delta x}{2D_D}$ | 0 | | $f_D$ | $k_{bBD}C_D(1) - k_{fBD}C_B(1)$ |
| 0 | 0 | $-\frac{k_{fCE}\Delta x}{2D_C}$ | 0 | $1 + \frac{k_{bCE}\Delta x}{2D_E}$ | | $f_E$ | $k_{bCE}C_E(1) - k_{fCE}C_C(1)$ |

---

# Reactions of Boron Heterocycles with Pyrazole[1]

C. Habben,[†] L. Komorowski,[‡,§] W. Maringgele,[†] A. Meller,*,[†] and K. Niedenzu*,[‡]

*Received December 28, 1988*

The interaction of pyrazole (=Hpz) with heterocycles containing two annular boron atoms generally seems to proceed by initial attack of the pyrazole NH moiety at the most basic site of the heterocycle. Subsequent reactions depend on the particular reaction conditions. For example, several pyrazaboles of the type RR′B($\mu$-pz)$_2$BRR′ (**1**) (**1a**, R = R′ = F from [(CH$_3$)$_2$NBF$_2$]$_2$ (C); **1b**, R = CH$_3$, R′ = pz from either (pz)(CH$_3$)B($\mu$-pz)B(pz)(CH$_3$) (**3a**) or CH$_3$B($\mu$-pz)($\mu$-NHCH$_3$)B($\mu$-NCH$_3$CSNCH$_3$)BCH$_3$ (Ic); **1c**, R = C$_2$H$_5$, R′ = pz from C$_2$H$_5$B[$\mu$-N(CH$_3$)$_2$]($\mu$-NCH$_3$CONCH$_3$)($\mu$-NCH$_3$CONHCH$_3$)BC$_2$H$_5$ (J)) and the type RB($\mu$-pz)$_2$($\mu$-X)BR (**2**) (**2a**, R = CH$_3$, X = NS(CH$_3$)$_2$N from HN($\mu$-BCH$_3$N)$_2$S(CH$_3$)$_2$ (H)) have been obtained. In addition, the following pyrazabole relatives of type **3** = (pz)RB($\mu$-pz)($\mu$-X)BR(pz) (**3a**, R = CH$_3$, X = NHCH$_3$ from CH$_3$N($\mu$-BCH$_3$NCH$_3$)$_2$Si(CH$_3$)$_2$ (F); **3b**, R = CH$_3$, X = NH$_2$ from S[$\mu$-BCH$_3$NSi(CH$_3$)$_2$]$_2$S (E); **3c**, R = C$_2$H$_5$, X = N(CH$_3$)$_2$ from C$_2$H$_5$B[$\mu$-N(CH$_3$)$_2$]($\mu$-NCH$_3$CONCH$_3$)($\mu$-NCH$_3$CONHCH$_3$)BC$_2$H$_5$ (J)) and the novel type **4** (general formula **5**) = RB($\mu$-pz)($\mu$-X)($\mu$-Y)BR (**4a**, R = C$_2$H$_5$, X = NHCH$_3$, Y = NCH$_3$CONCH$_3$ from CH$_3$N($\mu$-BC$_2$H$_5$NCH$_3$)$_2$CO (Ia); **4b**, R = C$_2$H$_5$, X = N(CH$_3$)$_2$, Y = NCH$_3$CSNCH$_3$ from J (see above); **4c**, R = CH$_3$, X = NHCH$_3$, Y = NCH$_3$CSNCH$_3$ from CH$_3$N($\mu$-BCH$_3$NCH$_3$)$_2$CS (Ic); **4d**, R = CH$_3$, X = NHC$_2$H$_5$, Y = NC$_2$H$_5$CSNC$_2$H$_5$ from C$_2$H$_5$N($\mu$-BCH$_3$NC$_2$H$_5$)$_2$CS (Id); **4e**, R = C$_6$H$_5$, X = NHCH$_3$, Y = NCH$_3$CSNCH$_3$ from CH$_3$N($\mu$-BC$_2$H$_5$NCH$_3$)$_2$CS (Ie)) have been isolated and characterized. The amine–borane complex (CH$_3$)H$_2$N·B(CH$_3$)(pz)$_2$ (**6**) was obtained from the reaction of either CH$_3$B($\mu$-NCH$_3$)($\mu$-NCH$_3$NCH$_3$)BCH$_3$ (G) or CH$_3$N($\mu$-BCH$_3$NCH$_3$)$_2$Si(CH$_3$)$_2$ (F) with Hpz.

## Introduction

There exist three principal types of neutral heterocyclic pyrazole (=Hpz) derivatives containing two four-coordinate annular boron

atoms. The pyrazaboles of type **1** have been known for more than 2 decades. The contain the skeleton >B($\mu$-pz)$_2$B<, and almost 100 different B- and/or C-substituted derivatives have been described.[2] Triply bridged pyrazaboles of type **2** with X = –OBRO–

---

[†] Georg August University.

[‡] University of Kentucky.

[§] On leave of absence from the Technical University of Wrocław, Wrocław, Poland.

(1) Boron–Nitrogen Compounds. 119 (K.N.). Part 118: Reference 19.

(2) Niedenzu, K.; Trofimenko, S. *Top. Curr. Chem.* **1986**, *131*, 1–37.